frontiers | Frontiers in Biomaterials Science

TYPE Original Research
PUBLISHED 06 February 2024
DOI 10.3389/fbiom.2024.1331032

OPEN ACCESS

EDITED BY
Valeria Chiono,
Polytechnic University of Turin, Italy

REVIEWED BY
Kang Tian,
Dalian Medical University, China
Iram Maqsood,
University of Maryland, United States
Thomas J. Kean,
University of Central Florida, United States

*CORRESPONDENCE
G. Lindberg,
Lindberg@uoregon.edu

RECEIVED 31 October 2023
ACCEPTED 03 January 2024
PUBLISHED 06 February 2024

CITATION
Lindberg G, Norberg A, Soliman B, Jüngst T, Lim K, Hooper G, Groll J and Woodfield T (2024), Fabrication of gelatin-heparin based cartilage models: enhancing spatial complexity through refinement of stiffness properties and oxygen availability.
Front. Front. Biomater. Sci. 3:1331032.
doi: 10.3389/fbiom.2024.1331032

Fabrication of gelatin-heparin based cartilage models: enhancing spatial complexity through refinement of stiffness properties and oxygen availability

G. Lindberg[1,2]*, A. Norberg[2], B. Soliman[2], T. Jüngst[3], K. Lim[2,4], G. Hooper[2], J. Groll[3] and T. Woodfield[2]

[1]Knight Campus for Accelerating Scientific Impact, University of Oregon, Eugene, OR, United States, [2]Department of Orthopaedic Surgery, University of Otago Christchurch, Christchurch, New Zealand, [3]Department of Functional Materials for Medicine and Dentistry and Bavarian Polymer Institute, University of Wuerzburg, Wuerzburg, Germany, [4]School of Medical Sciences, University of Sydney, Sydney, Australia

The intricate nature of native cartilage, characterized by zonal variations in oxygen levels and ECM composition, poses a challenge for existing hydrogel-based tissue models. Consequently, these 3D models often present simplified renditions of the native tissue, failing to fully capture its heterogenous nature. The combined effects of hydrogel components, network properties, and structural designs on cellular responses are often overlooked. In this work, we aim to establish more physiological cartilage models through biofabrication of photopolymerizable allylated-gelatin (GelAGE) and Thiolated Heparin (HepSH) constructs with tailorable matrix stiffness and customized architectures. This involves systematically studying how the native glycosaminoglycan Heparin together with hydrogel stiffness, and oxygen availability within 3D structures influence chondrogenic differentiation and regional heterogeneity. A comprehensive library of 3D hydrogel constructs was successfully developed, encompassing GelAGE-HepSH hydrogels with three distinct stiffness levels: 12, 55 and 121 kPa, and three unique geometries: spheres, discs, and square lattices. In soft GelAGE-HepSH hydrogels, the localization of differentiating cells was observed to be irregular, while stiff hydrogels restricted the overall secretion of ECM components. The medium-stiff hydrogels were found to be most applicable, supporting both uniform tissue formation and maintained shape fidelity. Three different 3D architectures were explored, where biofabrication of smaller GelAGE-HepSH spheres without oxygen gradients induced homogenous, hyaline cartilage tissue formation. Conversely, fabrication of larger constructs (discs and lattices) with oxygen gradients could be utilized to design heterogenous cartilage tissue models. Similarly, temporal oxygen gradients were observed to drive interconnected deposition of glycosaminoglycans (GAGs). Control samples of GelAGE without HepSH did not exhibit any notable changes in chondrogenesis as a function of stiffness, architectures, or oxygen concentrations. Overall, the incorporation of HepSH within GelAGE hydrogels was observed to serve as an amplifier for the biological effects from both stiffness and oxygen cues. In conclusion, fabrication of GelAGE-HepSH constructs designed to impose limitations on oxygen availability induce more zone-specific cartilage tissue alignment. This

systematic study of matrix components, network stiffness, and oxygen levels in 3D biofabricated structures contributes to the development of more physiologically relevant cartilage models while further enhancing our overall understanding of cartilage tissue engineering.

KEYWORDS

cartilage, bioinks, gelatin, heparin, stiffness, oxygen

1 Introduction

Amongst the ever-growing library of biomaterials used for tissue engineering and regenerative medicine (TERM) based approaches, gelatin hydrogels have consistently demonstrated efficacy as highly hydrated matrices for 3D cell culture (Klotz et al., 2016; Occhetta et al., 2015; Yue et al., 2015; Schuurman et al., 2013; Zhao et al., 2015). While examples include liver (Lewis et al., 2018; Wang et al., 2020; Lv et al., 2022), cardiac (McCain et al., 2014; Tijore et al., 2018), and bone (Chiesa et al., 2020; Leucht et al., 2020), one of the most common applications of gelatin hydrogels includes the encapsulation of chondrocytes within these hydrogels to fabricate cartilage tissue models (Klotz et al., 2016; Occhetta et al., 2015; Yue et al., 2015; Schuurman et al., 2013; Meng et al., 2019; Choi et al., 2019; Hölzl et al., 2022; Tsai et al., 2020; Pan et al., 2022). Gelatin hydrogels possesses several attractive features, such as their biocompatibility, tunable mechanical properties, and ability to support cellular functions crucial for tissue development. In efforts to better mimic the native hierarchically organized structure of cartilage (Sophia Fox et al., 2009; Huey et al., 2012; Boushell et al., 2017; Francis et al., 2018), a main focus of the past decade has been to converge these gelatin hydrogels with various additive manufacturing technologies (Klotz et al., 2016; Levato et al., 2020). This allows for the fabrication of complex 3D structures with precise control over construct shape, size and porosity. As such, rapid advancements of new constructs with microfiber-reinforced hydrogels have emerged as they are able to capture distinct mechanical zones of cartilage (Castilho et al., 2019; Steele et al., 2022). Despite these exciting advances in mechanical stability, cartilage 3D models still demonstrate a limited ability to replicate the heterogenous nature of the cartilage extra cellular matrix (ECM) (Lammi et al., 2018; Stampoultzis et al., 2021; Schäfer and Grässel, 2023). More specifically, cells are often unable to initiate zonal matrix deposition as the process relies on the intricate interaction between hydrogels and encapsulated cells (Lammi et al., 2018; Stampoultzis et al., 2021; Schäfer and Grässel, 2023).

Many of the physiological design criteria remain largely undefined due to the complexity and diversity of the cell interactions that occur in a hydrogel system. Specifically, the synergistic interplay between ECM molecules within the hydrogels, the stiffness of the gelatin hydrogel, and the localized presence of oxygen across different architectures. While hydrogels with stiffness values in the range of 1–30 kPa have often shown favorable outcomes in terms of chondrogenic differentiation *in vitro* (Levett et al., 2014; Wang et al., 2014; Visser et al., 2015; Visser et al., 2015; Li et al., 2016), the mechanism by which stiffness and ECM molecules can interplay to guide the formation of specific tissue regions remains understudied. For example, the incorporation of biological elements (e.g., glycosaminoglycans) in gelatin hydrogels is not consistently an efficient strategy to control the formation of cartilage tissue within *in vitro* models. Some studies demonstrating increased chondrogenesis following the inclusion of GAGs in gelatin hydrogels (Levett et al., 2014), while others report limited biological benefits with ECM matrix components (Visser et al., 2015). This variability is due to then many confounding parameters within the gelatin hydrogel system, especially stiffness (Martyniak et al., 2022). In addition, the sample architecture is often highly variable between different studies which may further affect the biological function of the ECM molecules within the hydrogel network. How these structural designs and network properties further correlate with downstream cellular access to oxygen is often overlooked (Rouwkema et al., 2010; Figueiredo et al., 2018). Unfortunately, the characterization of oxygen availability within 3D bioprinted, photopolymerized, structures is seldom reported on, primarily due to the complexities associated with analyzing or modelling oxygen in cell-laden hydrogels (Figueiredo et al., 2020). These factors include complex structures, heterogeneous crosslinking and mesh sizes, possible interactions between charged molecules, oxygen inhibition of free radical photopolymerization reactions, dynamic cellular oxygen consumption rates, enzymatic degradation of gelatin hydrogels, as well as static and dynamic cultures (Compañ et al., 1996; Malda et al., 2004; Bertlein et al., 2017; Axpe et al., 2019; Magliaro et al., 2019; Figueiredo et al., 2020). Furthermore, cellular activities and spatial reorganization is known to contribute to varying levels of oxygen exposure for chondrocytes (Zhou et al., 2004; Fathollahipour et al., 2018; Rogers and Meng, 2023). Importantly, dynamic oxygen fluctuations are often observed during the developmental or tissue maturation phase of cartilage as part of the continuous adaptation to the changes in mechanical and metabolic demands (Zhou et al., 2004; Rogers and Meng, 2023). Taken together, this underlines that the field of biomaterials and biofabrication still requires systematic investigation of the interplay between a range of these biological, physical, and structural properties and the downstream cellular functions in order to develop more physiological relevant *in vitro* cartilage models using hydrogels.

In this study, we aim to apply allylated gelatin (GelAGE) and a thiolated version of the ECM molecule Heparin (HepSH) as a versatile biomaterial platform with customizable stiffness and architectures to biofabricate cartilage models with more zone-like tissue heterogeneity. We seek to firstly incorporate HepSH in GelAGE as a bioactive component to drive cellular differentiation in the bioinks. We will herein systematically investigate the synergistic effects of covalent incorporation of bioactive HepSH with network stiffness and subsequent oxygen levels within biofabricated 3D structures on chondrogenesis. This provides a promising approach to engineer cartilage tissue models that more closely resemble the native tissue architecture, facilitating future studies on cartilage development, disease modelling, and drug screening.

2 Materials and methods

2.1 Materials and reagents

Gelatin (porcine skin, type A, gel strength 300), Heparin sodium salt (porcine intestinal mucosa, grade I-A), allyl glycidyl ether (AGE), 1-ethyl-3-(3-dimethylaminopropyl) carbodiimide (EDC), 1-hydroxybenzotriazole hydrate (HOBt), cysteamine, dialysis tubing cellulose membrane (MWCO 14 and 1 kDa), proteinase K, Trizma® base, ethylenediaminetetraacetic acid disodium salt dihydrate (Di-sodium-EDTA), 1,9-dimethyl-methylene blue zinc chloride double salt (DMMB), chondroitin-4-Sulfate, 4% neutral buffered formalin, glycine, sodium chloride (NaCl), phosphate buffered saline (PBS), sodium azide, hyaluronidase, ITS+1, L-proline, L-ascorbic acid-2-phosphate sesquimagnesium salt (AsAp), dexamethasone, fast green FCF, safranin-O, hydrochloric acid (37%), sodium hydroxide (NaOH), sodium bicarbonate, ß-mercapto-ethanol and primary antibody for Connexin43 (C6219) were all purchased from Sigma-Aldrich, St Louis, MO. 0.25% Trypsin-EDTA solution (with phenol red), CyQuant® cell proliferation assay kit, Gibco DMEM hi-glucose glutamax media, bovine serum albumin (BSA), Gibco 4-(2-hydroxyethyl)-1-piperazineethanesulfonic acid (HEPES), Gibco non-essential amino acids (NEAA), penicillin-streptomycin (10,000 U/mL and 10,000 µg/mL), Gibco fetal bovine serum (FBS), goat-anti-mouse secondary antibody (Alexa Fluor 488), 4,6-diamidino-2-phenylindole (D1306, DAPI), molecular probes calcein-AM and propidium iodide was obtained from Thermo Fisher Scientific, Auckland, NZ. Primary antibodies collagen II (II-II6B3-C) were acquired from DSHB, Iowa City, United States. Primary antibodies for collagen I (Ab34710) and aggrecan (ab3773) was obtained from Abcam, Melbourne, Australia. Transforming growth factor β-1 (TGFβ-1) was purchased from R&D systems, Minneapolis, United States. Type II collagenase (source: *Clostridium* histolyticum) was purchased from Worthington biochemical corporation, Lakewood, United States. Di-sodium hydrogen phosphate (NA2HPO4), acetic acid (glacial, 100%), and Gill's hematoxylin was purchased from Merck Millipore, North Shore City, NZ. Tissue-Tek® O.C.T Compound Sakura® Fintek was purchased from VWR International, Radnor, United States.

2.2 Macromer synthesis

HepSH and GelAGE were synthesized using protocols based on previously described methods (Bertlein et al., 2017; Brown et al., 2017). In short, Heparin was dissolved in PBS at 1 wt% and allowed to react with EDC, HOBt, and cysteamine, with 3.5-, 2.5-, and 3-fold molar excess over carboxylic groups, respectively. The pH was adjusted to 6.8 and the reaction was allowed to continue for 5 h at RT and was subsequently dialyzed (MWCO 14 kDa) against deionized water in order to remove unreacted molecules. Gelatin was dissolved in milliQ at 10 wt% and allowed to react with 12 mmol of AGE and 2 mmol NaOH per Gram of gelatin. The reaction was allowed to continue for 1 h at 65°C and the solution was dialyzed (MWCO 1 kDa) against deionized water. All macromer products were sterile filtered, lyophilized and stored at −20°C until use. The degree of modification (DoM), defined as the percentage of reactive groups that are modified, was determined using 1H-NMR and Ellman's assay according to previously described protocols (Nilasaroya et al., 2008; Benton et al., 2009; Bertlein et al., 2017; Brown et al., 2017; Soliman et al., 2020; Yang et al., 2021; Cui et al., 2022; Soliman et al., 2023).

2.3 Hydrogel fabrication

All hydrogel precursor solutions, as detailed in Table 1, were prepared by dissolving 20 wt% of GelAGE and 30–120 mM Dithiothreitol (DTT) in PBS supplemented with final photo-initiator concentrations of 1/10 mM Ru/SPS as previously described (Bertlein et al., 2017). To initiate cross-linking, the solutions were irradiated with 400–450 nm Vis-light (Rosco IR/UV filter equipped to OmniCure® S1500, Excelitas Technologies) for 3 min at 30 mW/cm^2 based on literature recommendations (Lim et al., 2016; Yang et al., 2021). All samples were photo-polymerized in an open environment (atmospheric oxygen). Fabrication of hydrogel discs were achieved by crosslinking the precursory solution in custom made silicone molds (ø5.5 mm and 2 mm deep).

2.4 Sacrificial bioprinting of fabrication of lattice structures

Extrusion printing was achieved with a Bioplotter (Sys + Eng, Germany) in a laminar-flow hood by extrusion of 30 wt% Pluronic®-F127 through a 23G (0.3 mm ID) needle. Pluronic®-F127 and the printing plate were set at 25°C and 30°C, respectively, by two separate Thermocube heating/cooling control loops (SSC Systems, NY, United States). Sterile Pluronic®-F127 stock solution was prepared through stirring vigorously overnight at 4°C followed by filtration (0.22 µm). Pluronic®-F127 was deposited in a layer-by-layer 0°–90° fashion into a 6-layered sacrificial template (12 × 12 mm) using 700 mm min^{-1} feed rate and 8 rpm auger speed; yielding ink filament size of 0.5 mm. Cell-laden GelAGE or GelAGE-HepSH precursor solutions were pipetted over the pluronic construct, filling the void in the template and generating positive filament imprints, followed by photo-initiated radical crosslinking as previously described. The constructs were washed with cold PBS (4°C, 10 min) to elute the sacrificial Pluronic structure. The residual polymerized hydrogel construct was transferred to fresh expansion media (DMEM hi-glucose glutamax media, 1% PenStrep, 10% FBS, and 0.1 mM AsAp), incubated at 37°C overnight and subsequently refreshed with chondrogenic differentiation media (DMEM hi-glucose glutamax media, 1% PenStrep, 1% ITS+, 0.2 mM AsAp, 0.1 µM Dexamethasone, 1.25 mg/mL BSA, and 10 ng/mL TGFβ).

2.5 Generation of spheres using microfluidics

A T-junction chamber served as a base for the microfluidic device, fabricated with clear resin on a Form2 SLA printer (Formlabs, Somerville, MA, United States) using 50 µm layers. All SLA-printed components were post-processed by washing twice in >95% isopropyl alcohol (IPA) for 10 min to ensure residual un-crosslinked resin was removed. The construct was

10.3389/fbiom.2024.1331032

TABLE 1 Hydrogel fabrication parameters.

ID	GelAGE	HepSH	DTT (mM)	Ru/SPS (mM)	Light (nm)	Intensity (mJ/cm^2)
GeIAGE-30	20wt%	0wt%	30	1/10	400–450	5400
GelAGE-60			60			
GelAGE-120			120			
GeIAGE-30-HepSH		0.05wt%	30			
GeIAGE-60-HepSH			60			
GelAGE-120-HepSH			120			

subsequently removed from the support material and post-cured with 320–500 nm light at 150 mW/cm^2 for 10–30 min (OmniCure® S1500). Sterile oil (canola oil) for the continuous phase was prepared by dry heat sterilization (3–4 h at 160°C) and was loaded in a 30 mL syringe (Terumo Luer Lock), injected perpendicular to the main axis of the T-junction using a Nylon male Luer integral lock ring to 1/4–28 UNF Thread (Value Plastics, CO, United States) and silicone washer to prevent leakage. A capillary of 660 µm outer diameter/530 µm inner diameter (Postnova Analytics, Germany) was fitted inside the channel of the T-Junction chamber and connected to a chemical resistant tubing (Tygon, Saint-Gobain, France) at the outlet side. The assembled fittings and tubes were all soaked in 96% EtOH overnight while the T-junction chamber was soaked in 70% EtOH for 10min, followed by rinsing and washing in sterile PBS prior to use. Cell-laden GelAGE or GelAGE-HepSH precursor solutions, prepared as previously described, was transferred into a 1 mL syringe (Terumo Luer Lock) and connected to the capillary on the microfluidic. Two syringe pumps (NE-300, New Era Instruments, United States) were applied to deliver 1,000 µL/mL and 50 µL/mL flow rates of the continuous and dispersed phase, respectively. The outlet tubing coil was placed under 400–450 nm light, and the spheres travelled through the tubing for 3 min, irradiated at 100 mW/cm^2 (Rosco IR/UV filter equipped to OmniCure® S1500). The effective time the spheres were exposed to the light was however 1 min as the area of light projection from the light guide was smaller than the tube coil. The fabricated spheres were collected and washed in PBS three times using centrifugation (500 x g, 3min) to remove residual oil.

2.6 Characterization of mass loss and swelling

After polymerization, casted disc hydrogels were weighed (m_{iw}) and three samples per hydrogel composition were directly lyophilized to record their initial dry weights (m_{id}) and determine the actual macromer weight fraction (m%), which is reported as the ratio of the initial dry weight to the initial weight.

$$m\% = \frac{m_{id}}{m_{iw}} \quad (1)$$

To determine the initial dry weight of the remaining samples, the factor of the actual macromer fraction and individual initial weight was used.

$$m_{id} = m\% \times m_{iw} \quad (2)$$

The remaining samples were allowed to swell in PBS solution, containing 0.1 wt% sodium azide, as an anti-microbial, at 37°C for 1 day. Swollen hydrogel samples were collected to record wet weight (m_s), then lyophilized to obtain the freeze-dried weight (m_d) and the mass loss and mass swelling ratio (q) was calculated according to the following calculations:

$$mass\ loss = 100\frac{m_{id} - m_d}{m_{id}} \quad (3)$$

$$q = \frac{m_s}{m_d} \quad (4)$$

The sol fraction of the hydrogels is defined as macromer not crosslinked into the hydrogel network and determined as the mass loss after equilibrium swelling (t = 1 day).

2.7 Quantification of Heparin retention in cell-free hydrogels

Following polymerization and incubation in PBS, containing 0.1 wt% sodium azide, at 37°C for 24 h, hydrogel samples were removed and digested at 56°C in 1 mg/mL proteinase K, dissolved in 10 mM Tris-HCl and 1 mM disodium EDTA solution. The PBS incubation liquid and its matching digested hydrogel sample were both allowed to react with DMMB to quantify the Heparin content. In brief, 50 µL of each sample and standard curve dilutions were transferred in triplicates to a 96-well microplate, to which 200 µL of DMMB solution was added and the absorbance was read at 520 nm (Thermo Scientific Varioskan Flash). Heparin content in both hydrogels (m_g) and surrounding PBS liquid (m_L) could be calculated from a matching standard curve generated by reacting known amounts of Heparin and HepSH with the DMMB agent. The retention, defined as the percentage of macromer not released to the surrounding liquid, could then be calculated for each time point using the following equation:

$$HepSH\ retention\ (\%) = 100\frac{m_g}{m_g + m_l} \quad (5)$$

Where m_g is the mass of Heparin macromers found in the digested hydrogels and m_l is the mass of Heparin macromers found leached out to the surrounding PBS that the corresponding hydrogel was submerged in.

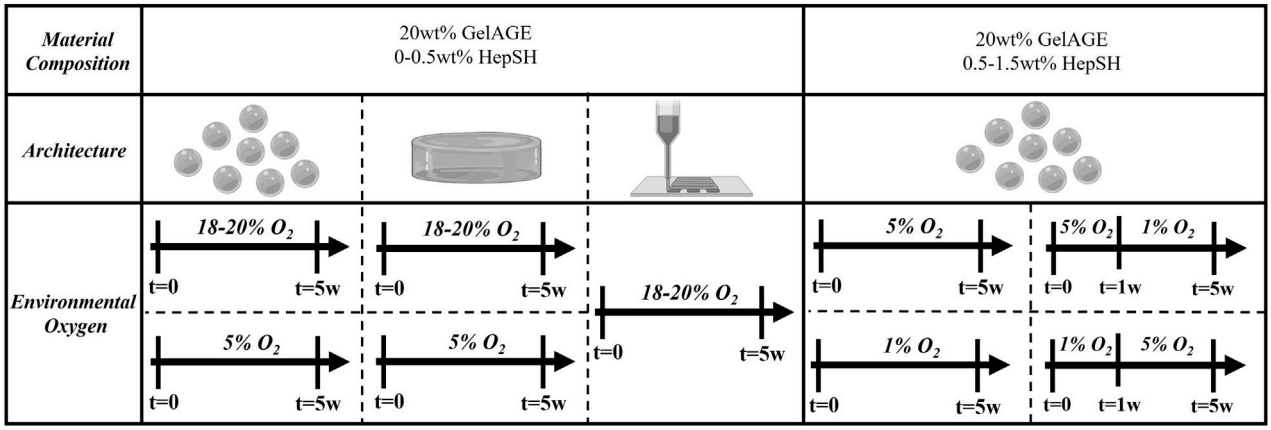

FIGURE 1
Schematic overview of the ambient culture conditions for cell-laden hydrogels investigated in the study. Concentration of HepSH, architecture and ambient oxygen settings was modulated to induce controlled cellular responses.

2.8 Cell isolation, expansion, and encapsulation

Chondrocytes were harvested from macroscopically normal regions of articular cartilage with consent from human patients undergoing ACL reconstruction (Health and Disability Ethics Committee New Zealand, URB/07/04/014/AM02). The tissue was collected from four donors (Sex: 3 female and 1 male, Age: 18–25 years, Ethnicity: 3 New Zealand European descent and 1 Māori descent) and digested in chondrogenic expansion media (DMEM hi-glucose glutamax media, 1% PenStrep, 10% FBS, and 0.1 mM AsAp) with 0.15% type II collagenase at 37°C in a humidified air incubator (set points: 5% CO_2, 21% O_2; actual: 5% CO_2, 18%–20% O_2) for 16–20 h. The solution was filtered through a cell strainer and isolated chondrocytes were expanded (525,000 cells per 175 cm^2 flask) into high-density monolayers for three passages cultured in chondrogenic expansion media and used for downstream cell culture experiments. Each experiment utilized cells from a single donor, and for each subsequent experimental repeat, a new donor was introduced to capture donor diversity across the collated results. The expanded chondrocytes were trypsinized (0.25% Trypsin in EDTA) and subsequently encapsulated in GelAGE and GelAGE-HepSH hydrogels as a single cell suspension at a concentration of 15×10^6 cells/mL. The cell-laden hydrogel constructs were cultured in chondrogenic differentiation media (DMEM hi-glucose glutamax media, 1% PenStrep, 1% ITS+, 0.2 mM AsAp, 0.1 µM Dexamethasone, 1.25 mg/mL BSA, and 10 ng/mL TGFβ) for up to 5 weeks to assess potential synergistic biological effects of hydrogel matrix components, stiffness, and architecture. Constructs were cultured at either hyperoxic (set points: 5% CO_2, 21% O_2, 37°C; actual: 5% CO_2, 18%–20% O_2, 37 °C) or physiological oxygen (physoxic/physioxic) conditions (5%–1% O_2, 5% CO_2, 37 °C), as outlined in Figure 1. Experiments with temporal oxygen settings included 15 ng/mL TGFβ in the chondrogenic differentiation media. Cell lockers™ with HEPA filters were used to enable culture without well plate lids to ensure rapid oxygen equilibration of the media following placement inside the incubators after media changes. Media was changed three times a week in atmospheric oxygen, with a maintained 0.37 cm media depth across all samples. Cell free hydrogels served as a negative control group across all experiments.

2.9 Mechanical testing and rheological evaluation

Compression testing was performed using a mechanical testing machine (MTS criterion 42, Australia) equipped with a 5N load cell. For compression tests, cylindrical samples (h = 2 mm, Ø = 5.5 mm) were loaded parallel to their long axis and tested at a constant cross head displacement rate of 0.01 mm s^{-1}. The compressive modulus was given by the slope of the stress-strain curve in the linear elastic range (strain: 10%–15%). The stress was calculated by normalizing the force to the original cross-sectional area of the sample (engineering stress). Rheological properties of the precursory solutions were furthermore characterized using a Physica MCR301 rheometer (Anton Paar, Germany), outfitted with a solvent trap and Peltier plate setup with a plate–plate geometry (25 mm diameter). All measurements were performed using rotational rheology (gap 0.2 mm).

2.10 Biochemical analysis

Cell-laden hydrogel constructs were collected after 1 day and 5 weeks of culture in chondrogenic differentiation media. Samples were washed in PBS, weighed, lyophilized, weighed again prior to digestion at 56°C in 1 mg/mL proteinase K, dissolved in 10 mM Tris-HCl and 1 mM disodium EDTA solution. The GAG content was quantified by allowing samples to react with the DMMB solution, as previously described (Lindberg et al., 2021). The absorbance was measured at 520 nm (Thermo Scientific Varioskan Flash). GAG content was calculated from a matching standard curve generated by reacting known amounts of chondroitin sulfate and subtracting the values obtained from cell-free controls. Both cell-free and cell-laden samples were diluted between 5–50 times to ensure detectability within the quantifiable linear range of the standard curve. Absorbance was measured immediately after addition of the

DMMB solution to the diluted samples and standards. Total DNA was quantified using CyQUANT® Cell Proliferation Assay Kit according to manufacturer's instructions and as described previously (Lindberg et al., 2021), following a pre-treatment of each sample with DNase-free RNase A (Thermo Fisher) to eliminate the RNA components of the fluorescent signal.

2.11 Histology and immunofluorescence examination

Cell-laden hydrogel constructs were collected after 5 weeks, washed with PBS, followed by fixation in 4% formaldehyde for 1 h at RT and washed in 0.3 M glycine in PBS to quench free aldehyde groups. The samples were then embedded in optimal cutting temperature compound (O.C.T) and cryo-sectioned into 30 µm thick sections. Haematoxylin, fast green, and Safranin-O was applied to visualize cell nuclei and extracellular GAGs to assess cartilaginous tissue formation. For immunohistological examination, sectioned samples were first incubated in 0.2% hyaluronidase for 30 min at RT and washed with PBS to reveal antigen epitopes. Constructs were subsequently blocked with 2% bovine serum albumin (BSA) in PBS for 30 min at RT. Primary antibodies for collagen I (1:200), collagen II (1:200), aggrecan (1:300), or connexin43 (1:200) were diluted in blocking buffer and applied for 3 h at RT. Samples were washed three times in blocking buffer for 10 min each followed by incubation with a goat-anti-mouse (Alexa Fluor® 488) and donkey-anti-rabbit (Alexa Fluor® 594) secondary antibodies, diluted in blocking buffer (1:400), in the dark for 1 h at RT. Constructs were washed a further three times with blocking buffer before incubation with blocking buffer containing 4′,6-Diamidino-2-Phenylindole, Dihydrochloride (DAPI, 1:1,000 dilution) in the dark for 10 min at RT. Lastly, constructs were washed three times in PBS and left hydrated. All images were captured using the Zeiss Axioimager Z1 microscope.

2.12 Oxygen measurements

An optical oxygen probe (Microx 4, NTH-PSt7 and Pt100, PresSensTM, Germany) was applied in accordance with manufactures instructions. The oxygen probe was connected to the in-house 3D printer (BioScaffolder, SysENG, Germany), fixated inside a commercially available luer-lock syringe, to gain precise control over z-height position during measurements. For physoxic samples (1%–5% O_2), manual measurements of the bottom and top of the constructs (no z-height control) were performed inside a hypoxia chamber (Whitley H35 hypoxiastation, Don Whitley Scientific, United Kingdom).

2.13 Statistical analyses

The data are presented as box plots, where whiskers represent the minimum and maximum value, the center-line represents the median, and the edges of the box represent the first and third quartiles. Each experiment was repeated with multiple sample replicates to study variability between samples, with detailed information about total n-values provided in each figure caption to clarify the size of each dataset. All samples have been collected using a simple random sampling and data was checked for outliers (ROUT method, Q = 1%). Additional assumptions of parametric analysis were validated using Shapiro-Wilk (alpha = 0.05) and Brown–Forsythe (alpha = 0.05) tests for normal distribution and equal variance, respectively. As an overview, differences between two groups or two time-points within the same group were assessed with unpaired t-tests (GraphPad Prism 10). *t*-test with Welsh correction was used for datasets that did not have equal variance while Mann Whitney U Tests were used for non-gaussian data sets. Differences between three or more groups were assessed by one-way ANOVA with Tukey *post hoc* analysis (GraphPad Prism 10). Kruskal–Wallis One-Way ANOVA were adopted for samples populations with non-gaussian distributions, while Brown-Forsythe and Welch ANOVA tests with Dunnett's Method were used for datasets with unequal variation. Ordinary two-way ANOVA with Tukey *post hoc* analysis (GraphPad Prism 10) was used for gaussian datasets with two or more variables investigated to determine synergistic effects. All two-way ANOVA tests were performed using a Geisser-Greenhouse correction, assuming non-equal variance (sphericity) between groups. Two-way ANOVA tests were only performed for two-variable data sets that were normally distributed. Differences between data points were considered significant when the probability of obtaining the difference by chance is less than 5%, this is defined as $p < 0.05$. The specific test used for individual data sets is detailed in each figure caption.

3 Results

3.1 Hydrogel and precursory properties

Photo-polymerization of GelAGE hydrogels was achieved using DTT as a thiolated crosslinker together with visible light photoinitiator system. Basic network characterization demonstrated a clear dose dependent response in solfraction, mass swelling ratios, HepSH retention, and mechanical properties, as a function of crosslinker concentration (Figures 2A–C). Covalent incorporation of HepSH was observed to reach near full conversion rates (Figure 2B). While reduced HepSH retention was detected in hydrogels crosslinked with the lowest crosslinker concentration, it should be noted that all conditions exhibited retention rates exceeding 88%. The polymerized hydrogels were categorized into three distinct stiffness categories: soft (12.0 ± 3.1 kPa), medium (54.9 ± 12.0 kPa), and stiff (121.0 ± 29.0 kPa). Additional investigation validated that neither the incorporation of HepSH or cells in GelAGE hydrogels influenced the mechanical properties (Figure 2C). The physiological characteristics of the precursory solutions prior to crosslinking is furthermore an important factor to consider for both tissue engineering and biofabrication applications. As seen in Figures 2D–E, the basic pH used during the GelAGE synthesis conditions results in gelatin fragmentation which enables a low-viscous bioink, even at a 20 wt% concentration. The physical characterization of the precursory solutions further reveals that the rheological properties of GelAGE were maintained across all investigated formulations. This decouples the need to optimize the printer settings between conditions. Long-term evaluation of mass loss, mass swelling ration and HepSH retention is detailed in Supplementary Figure S1.

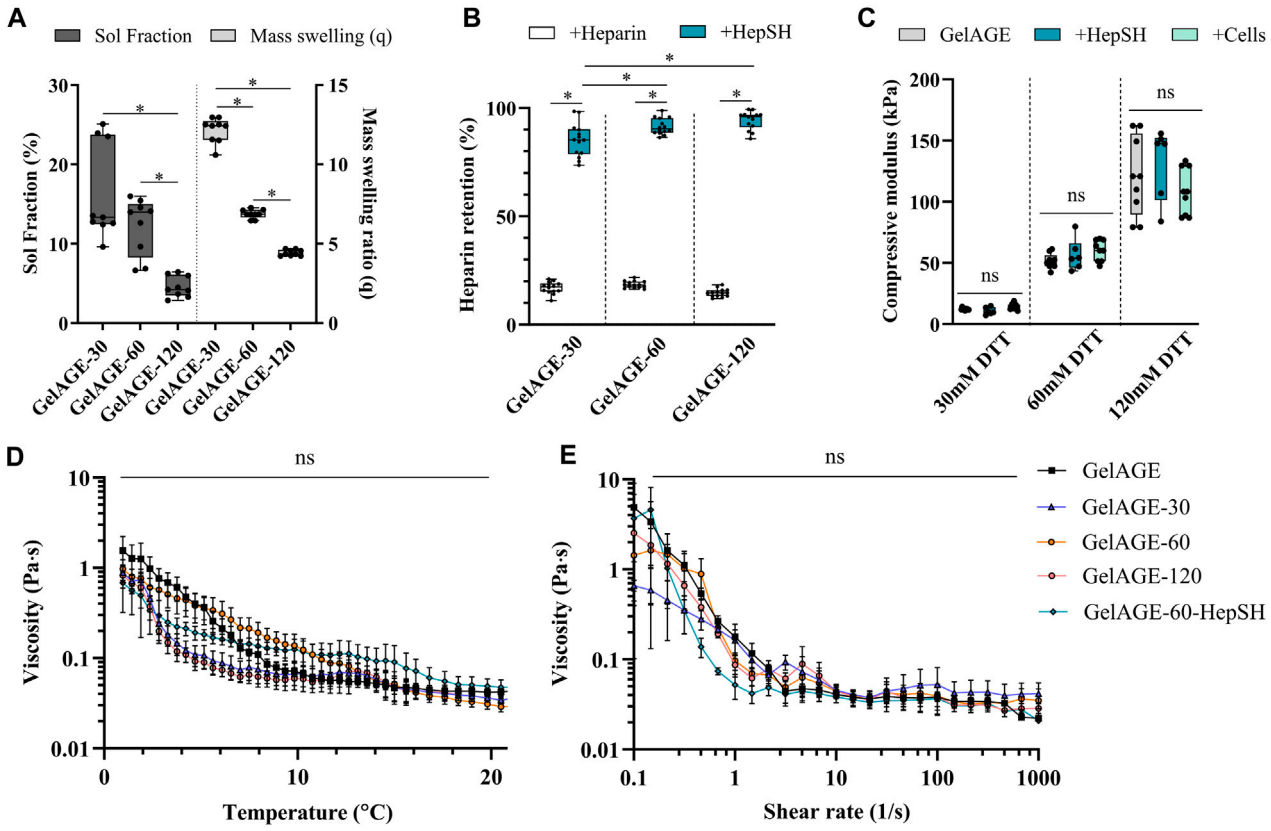

FIGURE 2
Overview of the physico-chemical properties [**(A)**; *n* = 9], covalent incorporation efficiency of HepSH [**(B)**; *n* = 14], and resultant mechanical properties [**(C)**; *n* = 12] of GelAGE hydrogels fabricated using different concentrations of thiolated crosslinker (DTT) after equilibrium swelling (24 h). Differences between groups were assessed by Kruskal-Wallice one-way ANOVA with Dunn's *post hoc* (sol fraction data), ordinary one-way ANOVA with *post hoc* Tukey analysis (mass swelling ratio data), or Brown-Forsythe and Welch corrected ANOVA tests with Tukey's *post hoc* test (Heparin retention data and compressive modulus data). **(A)** unpaired *t*-test with Welsh correction was performed to determine difference between HepSH and Heparin (controls) retention. * indicate significant differences ($p < 0.05$). Rheological assessment of various GelAGE formulations through temperature sweeps from 22°C–1°C **(D)** at 8s-i and strain sweeps from 0.1% to 1,000% at 4°C **(E)**, with *n* = 3 (one experimental repeat).

3.2 The effect of stiffness and HepSH on cellular function

Biochemical and histological techniques were applied to study the ECM secretion by chondrocytes encapsulated in hydrogel constructs with varying stiffness properties. GelAGE control hydrogels displayed an overall limited chondrogenic induction capacity. Results herein demonstrated that the conjugation of HepSH upregulated chondrogenesis (GAG/DNA) across all three stiffness conditions investigated as compared to GelAGE alone (Figure 3A). Both the soft (12 kPa) and medium (55 kPa) hydrogels displayed histologically detectable regions of pericellular GAG accumulation, as seen in the safranin-O and aggrecan stained sections (Figures 3B, C). All hydrogel conditions displayed positive connexin 43 staining, which is an indirect marker for cell-cell communication between neighboring cells. This suggested the possibility for coordinated responses to signaling cues within all evaluated hydrogel networks (Figure 3C). Moreover, a synergistic effect between softer network properties and HepSH containing hydrogels was quantified, displaying significantly higher GAG/DNA as compared to the stiffest hydrogel formulation (Figure 3A). It was however noted that the soft hydrogels displayed highly regional and heterogenous tissue formation, as evident by large standard deviations and irregular Safranin-O staining patterns. Encapsulated cells also proliferated significantly more in the softer hydrogels as compared to medium and stiff hydrogels (Supplementary Figure S2). The soft hydrogels furthermore lost their shape over time due to cell-driven material contraction (Supplementary Figure S3). Additional visualization of cell viability, collagen type I and II secretion, DNA quantification and mechanical properties is detailed in Supplementary Figures S2, S3.

3.3 The effect of architecture on oxygen availability

Our initial investigation focused on the fabrication of GelAGE-HepSH disc constructs with distinct stiffness properties and heights. Oxygen measurements verified that the oxygen availability within GelAGE constructs depended on both the hydrogel network stiffness and factors such as sample depth and cellular oxygen consumption (Figures 4A–C). Medium stiff (55 kPa) hydrogel structures with material thickness larger than 0.7 ± 0.3 mm were herein identified to display oxygen levels outside standardized atmospheric cell culture conditions (18%–21%) at the bottom (center) of the constructs. A

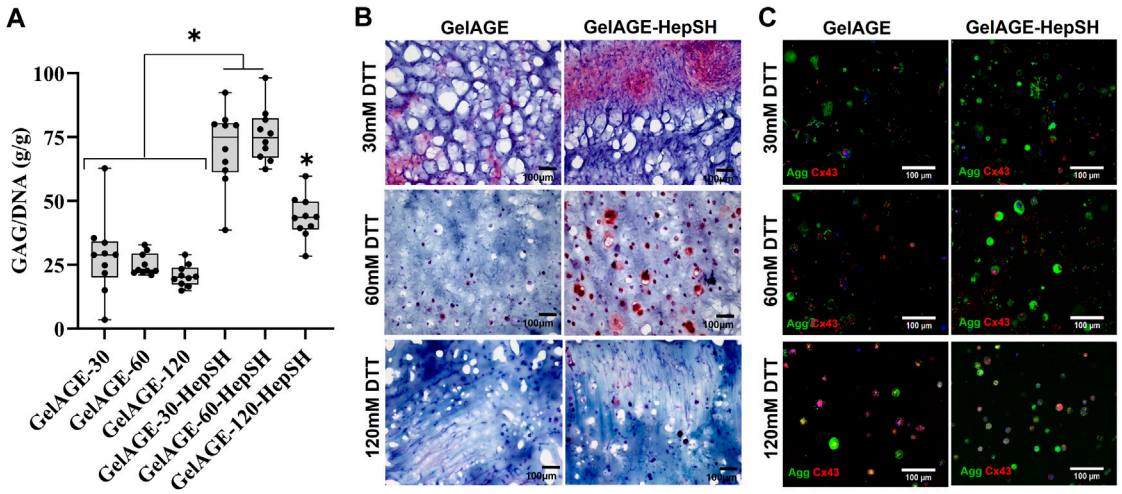

FIGURE 3
Quantification of GAG/DNA in cell-laden GelAGE and GelAGE-HepSH samples crosslinked with different DTT concentrations after 5 weeks of culture [**(A)**; $n = 10$]. Synergistic effects of crosslinker concentration (30–120 mM DTT) and addition of HepSH on GAG/DNA was evaluated using ordinary two-way ANOVA with *post hoc* Tukey analysis. * indicate significant differences ($p < 0.05$). Safranin-O **(B)** and Aggrecan/Connexin43 **(C)** stained sections of cells encapsulated in GelAGE and GelAGE-HepSH hydrogels after 5 weeks of culture. The cell experiments were carried out at atmospheric oxygen settings (18%–20% O_2). Scale bar = 100 μm.

distinct radial oxygen concentration gradient was also observed at the bottom of medium-stiff hydrogels (4 mm thick), in a *x-y* direction (Figure 4B). It was furthermore observed that seeding 15 million chondrocytes per ml of precursor solution yielded a significant reduction in localized oxygen concentrations only in constructs larger than 1.3 mm (Figure 4C). These results highlight that oxygen gradients through cell-laden hydrogels is a key factor to consider, and that each hydrogel formulation requires optimization of crosslinking conditions and architectures to control the local oxygen environment experienced by encapsulated cells.

3.4 The effect of oxygen availability (architecture) and HepSH on cellular function

As outlined in Figures 4D–F, GelAGE-HepSH spheres, discs, and porous lattice structures with medium stiffness (55 kPa) were successfully generated using three different fabrication techniques. Confirmation of cell viability can be found in Supporting Material (Supplementary Figure S4). The fabricated constructs were observed to increase in size post chondrogenic media incubation media and were characterized to have the following dimensions after equilibrium swelling (24 h): ø1.1 mm spheres, ø6 mm x 2.2 mm discs (diameter x height), and 15.2 × 15.2 × 2.6 mm lattice scaffolds (width x depth x height). It should herein be noted that although the lattice structures contain macro-pores, the continuous stacking in the junctions generates a series of identical square-shaped microenvironments in the x-y plane of 0.9 × 0.9 × 2.6 mm each (width x depth x height, Figure 4F). For GelAGE control hydrogels, results revealed no significant difference in matrix production between structural designs as the overall tissue formation remained limited (Figures 5A–B). A substantial increase in tissue formation was observed with the addition of HepSH across all three architectures. A strong synergistic effect between HepSH and constructs with oxygen gradients was further observed, promoting significant chondrogenesis in both the larger discs and lattice matrices as compared to the smaller spheres (ø1.1 mm, r = 0.55 mm). These findings are consistent with the oxygen gradients observed in the discs (Figure 4A), indicating that GelAGE-HepSH spheres with a radius below the identified 0.7 mm material thickness threshold does not generate oxygen gradients of biological significance. Both the gene expression of aggrecan and collagen type II in GelAGE-HepSH lattice constructs was confirmed to be upregulated within larger construct, supporting the formation of hyaline-like neo-cartilage (Figures 5C–F). Taken together, a noteworthy increase in both positive Safranin-O staining, quantitative GAG/DNA and Aggrecan gene expression confirmed that chondrogenesis was maximized in the largest constructs fabricated: GelAGE-HepSH lattices. These samples displayed a 50.1% increase in GAG/DNA and a 70.8% increase in Aggrecan gene expression as compared to semi-large constructs: GelAGE-HepSH discs. When GelAGE-HepSH lattices were compared directly to the smaller spheres (GelAGE-HepSH), the increase in GAG/DNA was more than double, while aggrecan gene expression was over 16-times higher. Additional biochemical quantification and immunohistological image analysis can be found in Supplementary Figure S4.

3.5 Fabricating 3D constructs that replicate natural oxygen gradients to guide tissue organization

To delve deeper into the combined effects of HepSH and 3D architectures on cellular development, we first utilized spheres as 3D models to study chondrogenesis under physiologically relevant oxygen conditions (5% O_2). Oxygen measurements verified that ø1.1 mm spheres maintained a consistent oxygen level throughout

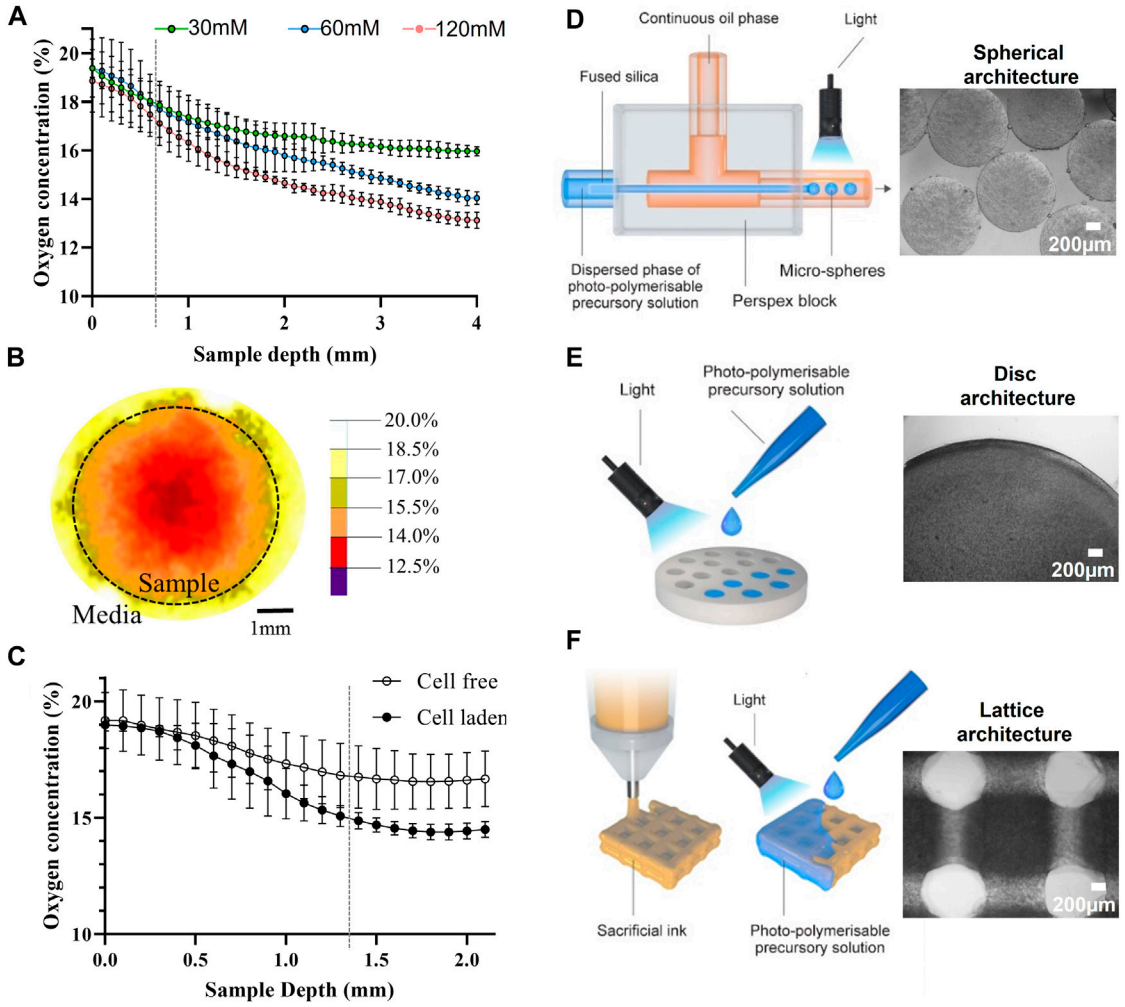

FIGURE 4
Characterization of oxygen concentration after equilibrium swelling (t = 24 h) in cell free GelAGE as a function of sample depth, grey line indicates when the 60 mM condition drops below 18% O_2 **(A)**. Oxygen concentration was also quantified as a function of sample width **(B)** and cells **(C)**, grey line indicates from which point the cell-laden constructs have significantly lower oxygen levels as compared to cell-free controls. For all oxygen experiments, *n* = 8 (three experimental repeats). The experiments were carried out at atmospheric oxygen settings (18%–20% O_2). Illustration of fabrication processes applied and bright-field images of GelAGE and GelAGE-HepSH constructs with distinct architectures **(D–F)**.

the 5-week culture period (Figure 6A). The construct's oxygen level matched the ambient conditions (5% O_2), confirming the absence of intricate oxygen gradients within the system. GelAGE-HepSH spheres thus yielded exceedingly homogenous cartilage tissue with a vast increase in GAG/DNA (66.5 ± 21.1 g/g) and chondrogenic markers as compared to pure GelAGE controls (Figures 6B–E). A significant upregulation of chondrogenesis in physoxic, 5% O_2, GelAGE-HepSH spheres was also observed in comparison to hyperoxic, 18%–20% O_2, spheres (controls), confirming the synergistic effect between HepSH and physiological oxygen levels (physoxia/physioxia) that is amplifying the cellular responses (Supplementary Figure S6).

To further investigate the effect of 3D architecture on long-term oxygen gradients and subsequent cellular developments, GelAGE-HepSH discs (ø6 mm, 2.2 mm height) was fabricated as a facile model system. Results confirm the successful formation of a natural spatial oxygen gradient that range between 5%–1% O_2 from top to bottom of the construct (Figure 6A). The spatial oxygen gradients in the disc constructs diminished over time (1day = 0.9–5.0% O_2, 5w = 3.9–5.0% O_2). The cells closer to the surface thus experience a constant level of 5% O_2, while cells closer to the bottom experienced fluctuating oxygen levels. Results herein revealed that these dynamic oxygen gradients induce a more zone-like GAG accumulation and orientation (Figure 6D). Specifically, safranin-O-stained sections confirmed more GAGs accumulating in the O_2-deprived regions at the bottom of the constructs as compared to the surface regions. Histological observations also showed variations in cellular localization, where cells in the lower regions tended to accumulate and stack along the lateral *z*-axis with highly organized GAG secretion. Conversely, cells in the middle and upper regions displayed a more random distribution, accumulating GAGs in a more rounded configuration (Figure 6D). Taken together, the design of GelAGE-HepSH constructs with larger architectures promotes dynamic oxygen gradients and subsequently zone-like cartilage tissue deposition under physiologically relevant oxygen settings.

10.3389/fbiom.2024.1331032

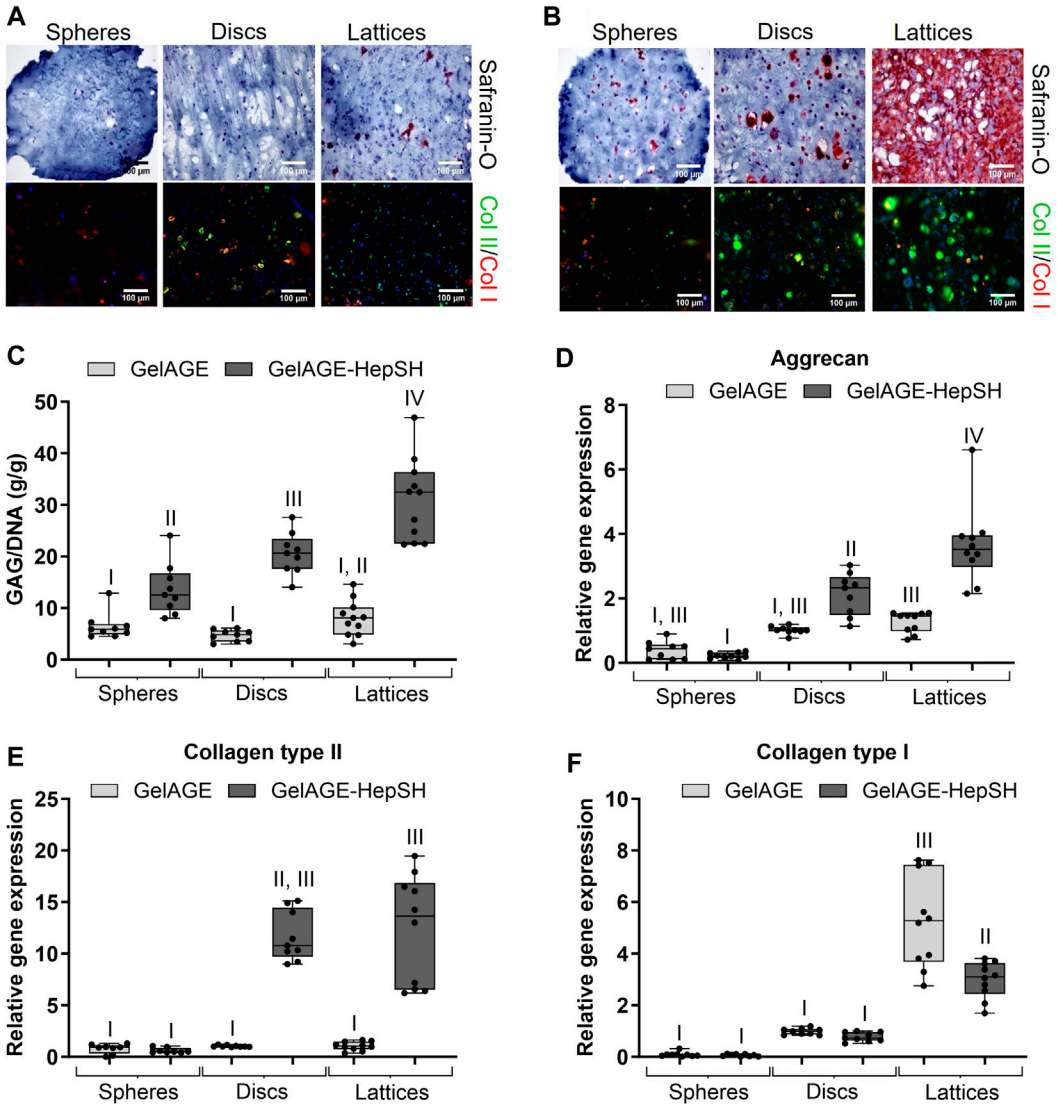

FIGURE 5
Safranin-O stained and Collagen type II/I stained sections of cells encapsulated in medium-stiff GelAGE **(A)** and GelAGE-HepSH **(B)** hydrogels with different architectures after 5 weeks of culture (three experimental repeats). Scale bar = 200 μm. Quantification of GAG/DNA **(C)**, with $n_{spheres}$ = 9 (10 spheres pooled per analytical sample, $n_{spheres,\ total}$ = 90), n_{Discs} = 9, and $n_{Lattices}$ = 11. Aggrecan **(D)**, Collagen type II **(E)**, and Collagen type I **(F)** gene expression in cell-laden GelAGE and GelAGE-HepSH constructs), with: $n_{spheres}$ = 8 (10 spheres pooled per analytical sample, $n_{rispheres,\ total}$ = 80), n_{Discs} = 9, and $n_{Lattices}$ = 10. Differences between groups were assessed by an ordinary two-way ANOVA with *post hoc* Tukey analysis to study the synergistic effects of crosslinker concentration (30–120 mM DTT) and addition of HepSH on biological outcomes. Groups without the same roman number indicate significant differences ($p < 0.05$). The experiments were carried out at atmospheric oxygen settings (18%–20% O_2).

3.6 The synergistic effects of temporal physoxia and HepSH

To explore the possibility of tailoring and customizing the synergistic biological effects of GelAGE-HepSH hydrogels and dynamic oxygen gradients, we conducted experiments to investigate whether altering the concentrations of HepSH and/or varying ambient oxygen settings over time could be used to initiate zonal matrix deposition in smaller constructs. Investigating temporal oxygen gradients is also of importance in order to better reflect the inherent variations in cartilage oxygen levels that can occur as a result of daily activity and rest cycles (Zhou et al., 2004; Rogers and Meng, 2023). We utilized spheres as 3D models to remove spatially confounding factors and study chondrogenesis under physiologically relevant and temporally varied oxygen conditions (1%–5% O_2). Results confirmed that increasing HepSH content from 0.5 wt% to 1.5 wt % significantly improved chondrogenic differentiation within cell-laden spheres cultured at 5% O_2 (Figures 7A, B). A similar dose-dependent HepSH response was observed for spheres with a temporally dynamic oxygen gradient, either moving from 1%–5% O_2 or from 5%–1% O_2 over the 5-week culture period (Figure 7A). Histological evaluation further reveals that constructs exposed to temporal oxygen gradients,

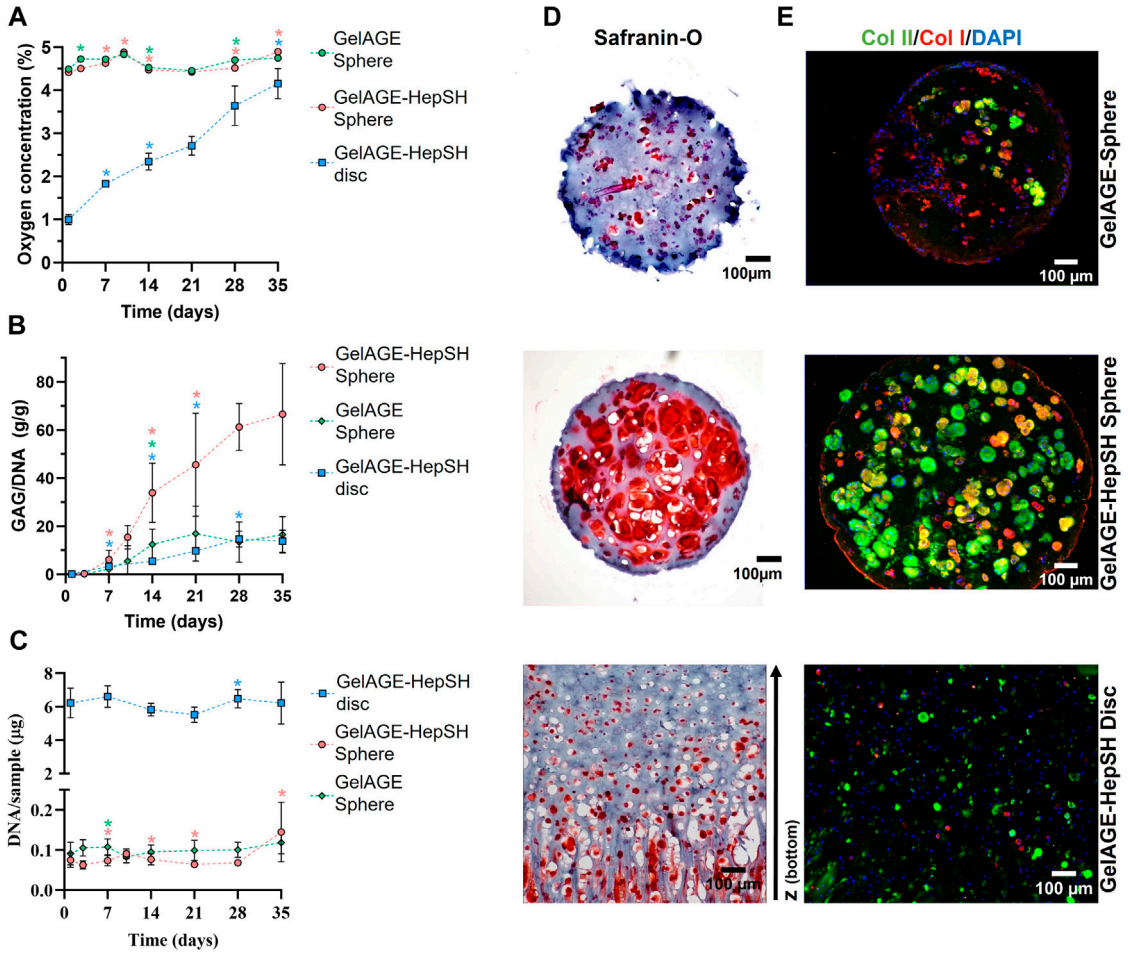

FIGURE 6
Quantification of oxygen concentration [**(A)**; *n* = 15], GAG/DNA [**(B)**; *n* = 9] and DNA [**(C)**; n = 9) in cell-laden GelAGE and GelAGE-HepSH constructs (three experimental repeats). Error bars represent the mean ± SD. Differences between two time-points within the same groups were assessed with multiple unpaired t-tests, where *indicates significant difference at that time-point as compared to the previous time-point ($p < 0.05$). The color of the asterisk denotes the condition with a statistical significance. Safranin-O stained sections of cells encapsulated in GelAGE and GelAGE-HepSH hydrogels with different architectures after 5 weeks of physoxic culture **(D)**. Immunofluorescent analysis of GelAGE samples following culture in chondrogenic differentiation media to visualize the cell nuclei, Collagen type I and type II **(E)**. Scale bar = 100 µm. The experiments were carried out at physoxic oxygen settings (5% O_2).

either high-low or low-high, have large pericellular regions stained positive with safranin-O (Figure 7B). These results corroborate the synergistic effect between HepSH and temporal oxygen gradients to induce interconnected secretion of sGAGs within gelatin-based hydrogels.

4 Discussion

This study explores the intricate interplay between bioactive HepSH, network stiffness, and oxygen levels within 3D gelatin hydrogel structures. Our initial investigation focused on the feasibility of designing thiol-ene clickable GelAGE-HepSH hydrogels with controllable network properties. Our findings of high HepSH incorporation efficiency align with previous reports around the application of thiol-ene click chemistry, known to allow for high conversion rates (Hoyle et al., 2010; Lowe, 2014; Fairbanks et al., 2017). Our results report limited dimensional and physico-chemical changes between cell-laden and cell-free hydrogels, similar to other thiol-ene based crosslinking systems (Fairbanks et al., 2009; Roberts and Bryant, 2013; Greene and Lin, 2015). This is a major advantage over commonly applied hydrogel platforms which often observe a significant reduction (30%–50%) in mechanical properties following the addition of cells (Bryant and Anseth, 2002; Peter et al., 2014; Mouser et al., 2016). Principally, it comes down to the ability of thiol-ene systems to still propagate even when radicals are scavenged, otherwise causing a decay and ultimately limiting the formation of crosslinks (Cramer et al., 2003; Hoyle et al., 2004; Hoyle and Bowman, 2010; Lobo et al., 2010; Roberts and Bryant, 2013; Zavada et al., 2014; Mouser et al., 2016).

Further examination of the precursor solution emphasizes that the synthesized GelAGE bioink exhibits low viscosity, even at a concentration of 20 wt%. This characteristic renders it highly suitable for applications using microfluidics as well as sacrificial

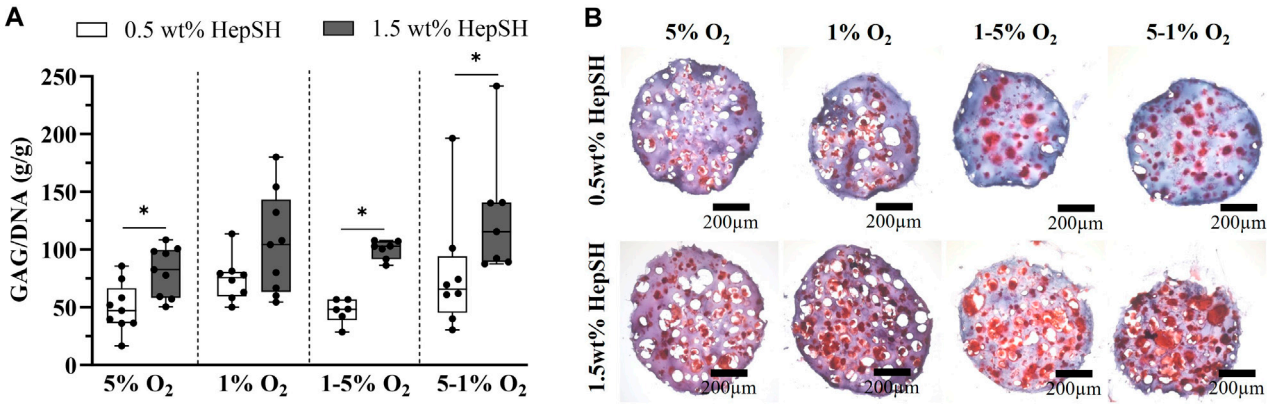

FIGURE 7
Quantification of GAG/DNA in cell-laden GelAGE-HepSH constructs **(A)**; n = 6–9, three experimental repeats). Error bars represent the mean ± SD of 5-9 samples (three experimental repeats). Differences between groups were assessed by a Mann Whitney U Tests analysis to study differences between HepSH concentration within each group. A Kruskal-Wallice one-way ANOVA with Dunn's *post hoc* was used to evaluate the effect of oxygen levels for each material formulation. *indicates significant difference ($p < 0.05$). Safranin-O stained sections of cells encapsulated in GelAGE-HepSH hydrogels with different concentrations of HepSH (0.5wt% and 1.5wt%) after 5 weeks of culture under variable oxygen concentrations **(B)**. Scale bar = 200 µm. The experiments were carried out at dynamic physoxic oxygen settings (1%, 5%, 1%–5% and 5%–1% O_2).

bioprinting, as explored in the context of this study. The bioink's low viscosity also at a higher concentration enhances its versatility, making it applicable to various techniques and settings in the field of biofabrication. As tailoring GelAGE stiffness and bioactivity does not herein significantly affect the rheological properties, it thus removes the need to anew identify the fabrication window for each individual formulation through an otherwise long and iterative process (Bertlein et al., 2017).

Through systematic investigation of chondrogenesis in soft, medium-stiff and stiff GelAGE-HepSH hydrogels, it was confirmed that hydrogels in a range between 15–50 kPa are particularly effective in facilitating chondrogenic development. Our observations that HepSH enhances cellular responses to stiffness as a microenvironmental cue has not been previously reported. However, the observation of limited ECM secretion in our 120 kPa stiff hydrogels corresponds well with literature reports suggesting that matrix production in stiffer hydrogels is restricted to the pericellular region simply due to space limitations (Bian et al., 2013; Levett et al., 2014; Wang et al., 2014; Visser et al., 2015; Li et al., 2016; Mouser et al., 2016). It should be noted that we observed that the soft GelAGE-HepSH constructs were not able to maintain their shape over time (Supporting Material). This structural deformation over time ultimately limits the application of softer GelAGE-HepSH hydrogels for the fabrication of 3D structures with controllable architectures. In this study, it was thus argued that medium-stiff GelAGE-HepSH hydrogels were the most attractive hydrogel formulation to further model various structure-function relationships. Taken together, this formulation allows efficient crosslinking and shape stability while supporting paracrine signaling, limiting fibroblastic like proliferation while preserving both homogenous proteoglycan and collagen type II accumulation.

To map the intricate correlations between HepSH, stiffness and 3D architectures, we first characterized the effect of architecture on localized oxygen availability. Oxygen measurements confirmed that oxygen availability within photo-polymerizable GelAGE constructs depended on network stiffness, sample depth, and cellular oxygen consumption. While some studies have explored adaptation systems such as perfusion culture systems and microchannel constructs to mitigate oxygen diffusion limitations in large hydrogel constructs, a notable gap in the literature revolves around quantitatively assessing the actual oxygen levels within these systems (Mavris and Hansen, 2021). Some tissue engineering and biofabrication strategies operate under the general assumption that the same principle for oxygen diffusion limits within human tissues (approximately 100–200 µm) hold true also in engineered tissue constructs (Starling, 1923; Carmeliet and Jain, 2000; Rouwkema et al., 2010). However, our findings challenge this widespread assumption and are reinforced by recent research utilizing gelatin methacryloyl, which emphasized substantial oxygen diffusion limitations also in very soft hydrogels (<0.25 kPa) (Schmitz et al., 2022). Others have reported findings around how hydrogel thickness influence the oxygen availability in hydrogels (Rouwkema et al., 2010; Figueiredo et al., 2018; Figueiredo et al., 2020; Mavris and Hansen, 2021). Interestingly, our additional findings indicate that cellular oxygen consumption becomes less relevant in smaller constructs. This observation is also supported by the work of others. For example, Schmitz and colleagues conducted a study affirming that the presence of 5 million stromal cells per milliliter does not induce significant changes in oxygen levels within soft gelatin hydrogels (Schmitz et al., 2022).

Our results further confirmed unique cellular responses to various architectural configurations and the synergistic effects of covalently incorporated thiolated Heparin in gelatin hydrogels–which has previously never been reported on. Specifically, the results provide compelling evidence for the increased chondrogenesis in GelAGE-HepSH lattice structures. This included a 50% and 116% increase in GAG/DNA for the larger lattices as compared to discs and spheres, respectively. The aggrecan gene expression in GelAGE-HepSH lattices was particularly striking, with a 16-fold higher expression level than seen for the smaller spheres. This size dependent increase in chondrogenesis in synergy with HepSH suggest that the structural

characteristics of GelAGE-HepSH contribute significantly to the promotion of chondrogenic outcomes.

These collective findings highlight the critical importance of considering the role both architectural parameters and hydrogel composition have on the local oxygen tension within thiol-ene clickable cell-laden constructs. In the realm of cellular biology and the effects of hypoxia, a significant focus has been on the activation of transcription factors like HIF-1 and HIF-2. These transcription factors play a crucial role in regulating changes in gene expression driven by oxygen availability. Notably, prior research has demonstrated that HIF has the capability to suppress the activity of endosulfatase-1 (HSulf-1) (Khurana et al., 2011), which function is to otherwise remove sulfate moieties on native sGAG, such as Heparin. Future studies should thus consider investigating HIF-1α dependent downregulation of the HSulf-1 enzyme within Heparin-rich gelatin hydrogels.

As oxygen is known to be a powerful regulatory molecule that dictates cellular responses, it was furthermore explored if customizing the scaffold architecture of GelAGE-HepSH could be used as a strategy to mimic the native oxygen gradients present in cartilage to help induce zonal cartilage structures. Physoxia for cartilage ranges from approximately 1%–10%, depending on, e.g., spatial location, thickness of the tissue, cellular oxygen consumption, cell density and mechanical stimulation (Zhou et al., 2004). It is worth noting that the average thickness of articular cartilage in the human joint is approximately 1.5 mm. This dimension exhibits slight regional variations, reportedly measuring between 1.0–1.62 mm in ankle joints while it ranges from 1.69–2.55 mm in knee joints (Shepherd and Seedhom, 1999).

Results confirm the successful formation of a natural oxygen gradient between 5%–1% from top to bottom of the GelAGE-HepSH hydrogels when using larger 2.2 mm constructs. In addition to the spatial variability, the constructs also displayed a temporal change in the local oxygen concentrations over the 5-week culture period. These dynamic, spatio-temporal, oxygen gradients were herein successfully shown to induce zonal-like GAG secretion and orientation while ø1.1 mm spheres without spatial or temporal oxygen levels instead enabled homogenous tissue formation. Previous reports have similarly shown that both cell distribution and tissue growth can be heterogeneous across large hydrogel structures cultured under static conditions (Brown et al., 2017; Lalitha Sridhar et al., 2017), often suggesting a correlation with material thickness and passive diffusion of, e.g., oxygen, nutrients and waste products (Colom et al., 2014; Figueiredo et al., 2018). In engineered hydrogel systems relying on passive diffusion, it has been shown that cells deplete oxygen prior to glucose (Colom et al., 2014; Figueiredo et al., 2018), which suggest that oxygen availability is the main factor altering the cellular responses in *z*-direction rather than nutrient availability. To confirm these findings, we utilized ø1 mm spheres, without spatial differences in oxygen availability, to precisely control the temporal oxygen levels by simply altering the ambient conditions. Interestingly, cells cultured under temporal oxygen settings displayed large regions of GAG deposition with high interconnectivity and density. This was particularly evident in the high HepSH concentration (1.5 wt%) with dynamic 5%–1% O_2 levels. Additionally, the inclusion of higher HepSH significantly improved chondrogenesis across most oxygen settings investigated, except for the 1% static oxygen tension. It thus appears that biological benefits can be achieved either through increased HepSH concentration or through exposure to physoxic oxygen settings. As such, it should be noted that all conditions represented in Figure 7 are in the physoxic range and capable of stimulating cells to produce noteworthy GAG deposition. Within these physoxic environments, whether dynamic or static, there was no significant differences observed in GAG/DNA between distinct oxygen levels. This may be due to the binary switch between two oxygen levels within this model, as opposed to the gradual and natural shift observed within larger disc constructs over the 5-week culture period (Figure 6). Previous literature has shown that the use of micromass pellets (biomaterial free) to generate cartilage *in vitro* relies heavily on a natural spatial-temporal oxygen gradient that forms during culture, progressively transitioning over time (Li et al., 2014). This is in line with previous literature findings highlighting the beneficial biological effects of conducting cartilage cultures in lower oxygen settings, often correlated with the oxygen-sensitive HIF-1 and HIF-2 (Gultice et al., 2009; Lekvijittada et al., 2021). As such, further studies into the role of HIF1α′s interplay with dynamic oxygen levels and Heparin are warranted. Taken together, our findings underscore that there is an intricate relationship between oxygen availability, HepSH concentration, and the resulting matrix deposition characteristics.

5 Conclusion

This study introduces GelAGE-HepSH as a versatile hydrogel platform that enables simultaneous manipulation of the physical environment and structural characteristics. The efficient incorporation of bioactive Heparin, with nearly complete retention, promotes chondrogenesis in hydrogels with a wide range of stiffnesses and diverse architectural designs. Medium-stiff GelAGE-HepSH hydrogels herein provided the most attractive microenvironment for both proteoglycan and type II collagen matrix accumulation while maintaining construct shape throughout the culture period. Additionally, the study uncovers a synergy between HepSH and the oxygen gradients present in different hydrogel architectures, facilitating the fabrication of cartilage with either homogeneous or zone-specific tissue organization. Specifically, fabrication of photo-polymerized GelAGE-HepSH constructs that impose limitations on oxygen availability, using a stiffness range of 50 kPa and material thickness exceeding 0.7 mm, induce more zone-specific cartilage tissue alignment. Conversely, by designing GelAGE-HepSH hydrogels with spatial and/or temporal oxygen gradients offers unique opportunities to manipulate the secretion of GAGs. Conversely, when designed with dynamic oxygen conditions, spanning between 1%–5% O_2, GelAGE-HepSH hydrogels promote the formation of GAG regions that exhibit great interconnectivity and density, mirroring some of the matrix characteristics typically found in the middle and deep cartilage zones.

Overall, our study provides comprehensive insights into the interplay of bioactive ECM components, hydrogel network properties, and architectural features that modulate oxygen levels, and thereby collectively guide cellular behaviour and tissue organization. As the field of cartilage TERM moves forward, the need for hydrogels that can

combine the synergistic benefits of biochemical and structural cues to fabricate more mimetic tissue analogues is apparent. This requires continued identification of essential relationships between cellular functionality and intricate design parameters.

Data availability statement

The original contributions presented in the study are included in the article/Supplementary Material, further inquiries can be directed to the corresponding author.

Ethics statement

The studies involving humans were approved by the Health and Disability Ethics Committee New Zealand. The studies were conducted in accordance with the local legislation and institutional requirements. The participants provided their written informed consent to participate in this study.

Author contributions

GL: Conceptualization, Data curation, Formal Analysis, Funding acquisition, Investigation, Methodology, Project administration, Resources, Software, Supervision, Validation, Visualization, Writing–original draft, Writing–review and editing. AN: Data curation, Writing–original draft, Writing–review and editing. BS: Data curation, Methodology, Writing–review and editing. TJ: Methodology, Writing–review and editing. KL: Supervision, Writing–review and editing. JH: Supervision, Writing–review and editing. JG: Methodology, Supervision, Writing–review and editing. TW: Methodology, Supervision, Writing–review and editing.

Funding

The author(s) declare financial support was received for the research, authorship, and/or publication of this article. The authors acknowledge funding by New Zealand Health Research Council Emerging Researchers First grants 19/679 (GL) and Explorer 21/802 (GL), the University of Otago Health Sciences Postdoctoral Fellowship (GL), the Knight Campus for Accelerating Scientific Impact (start-up support, GL) and the Wu Tsai Human Performance Alliance (Moonshot grant, GL).

Conflict of interest

The authors declare that the research was conducted in the absence of any commercial or financial relationships that could be construed as a potential conflict of interest.

Publisher's note

All claims expressed in this article are solely those of the authors and do not necessarily represent those of their affiliated organizations, or those of the publisher, the editors and the reviewers. Any product that may be evaluated in this article, or claim that may be made by its manufacturer, is not guaranteed or endorsed by the publisher.

Supplementary material

The Supplementary Material for this article can be found online at: https://www.frontiersin.org/articles/10.3389/fbiom.2024.1331032/full#supplementary-material

References

Axpe, E., Chan, D., Offeddu, G. S., Chang, Y., Merida, D., Hernandez, H. L., et al. (2019). A multiscale model for solute diffusion in hydrogels. *Macromolecules* 52, 6889–6897. doi:10.1021/acs.macromol.9b00753

Benton, J. A., DeForest, C. A., Vivekanandan, V., and Anseth, K. S. (2009). Photocrosslinking of gelatin macromers to synthesize porous hydrogels that promote valvular interstitial cell function. *Tissue Eng. Part A* 15, 3221–3230. doi:10.1089/ten.tea.2008.0545

Bertlein, S., Brown, G., Lim, K. S., Jungst, T., Boeck, T., Blunk, T., et al. (2017). Thiol-ene clickable gelatin: a platform bioink for multiple 3D biofabrication technologies. *Adv. Mater* 29. doi:10.1002/adma.201703404

Bian, L., Hou, C., Tous, E., Rai, R., Mauck, R. L., and Burdick, J. A. (2013). The influence of hyaluronic acid hydrogel crosslinking density and macromolecular diffusivity on human MSC chondrogenesis and hypertrophy. *Biomaterials* 34, 413–421. doi:10.1016/j.biomaterials.2012.09.052

Boushell, M. K., Hung, C. T., Hunziker, E. B., Strauss, E. J., and Lu, H. H. (2017). Current strategies for integrative cartilage repair. *Connect. Tissue Res.* 58, 393–406. doi:10.1080/03008207.2016.1231180

Brown, G. C. J., Lim, K. S., Farrugia, B. L., Hooper, G. J., and Woodfield, T. B. F. (2017). Covalent incorporation of heparin improves chondrogenesis in photocurable gelatin-methacryloyl hydrogels. *Macromol. Biosci.* 17, 1700158. doi:10.1002/mabi.201700158

Bryant, S. J., and Anseth, K. S. (2002). Hydrogel properties influence ECM production by chondrocytes photoencapsulated in poly(ethylene glycol) hydrogels. *J. Biomed. Mater Res.* 59, 63–72. doi:10.1002/jbm.1217

Carmeliet, P., and Jain, R. K. (2000). Angiogenesis in cancer and other diseases. *Nat. Lond.* 407, 249–257. doi:10.1038/35025220

Castilho, M., Mouser, V., Chen, M., Malda, J., and Ito, K. (2019). Bi-layered micro-fibre reinforced hydrogels for articular cartilage regeneration. *Acta Biomater.* 95, 297–306. doi:10.1016/j.actbio.2019.06.030

Chiesa, I., De Maria, C., Lapomarda, A., Fortunato, G. M., Montemurro, F., Di Gesù, R., et al. (2020). Endothelial cells support osteogenesis in an *in vitro* vascularized bone model developed by 3D bioprinting. *Biofabrication* 12, 025013. doi:10.1088/1758-5090/ab6a1d

Choi, J. R., Yong, K. W., Choi, J. Y., and Cowie, A. C. (2019). Recent advances in photo-crosslinkable hydrogels for biomedical applications. *BioTechniques* 66, 40–53. doi:10.2144/btn-2018-0083

Colom, A., Galgoczy, R., Almendros, I., Xaubet, A., Farré, R., and Alcaraz, J. (2014). Oxygen diffusion and consumption in extracellular matrix gels: implications for designing three-dimensional cultures. *J. Biomed. Mater. Res. Part A* 102, 2776–2784. doi:10.1002/jbm.a.34946

Compañ, V., Román, J., Riande, E., Sørensen, T., Levenfeld, B., and Andrio, A. (1996). Oxygen transport through methacrylate-based hydrogels with potential biological capability. *Biomaterials* 17, 1243–1249. doi:10.1016/0142-9612(96)84945-3

Cramer, N. B., Reddy, S. K., O'Brien, A. K., and Bowman, C. N. (2003). Thiol–Ene photopolymerization mechanism and rate limiting step changes for various vinyl functional group chemistries. *Macromolecules* 36, 7964–7969. doi:10.1021/ma034667s

Cui, X., Alcala-Orozco, C. R., Baer, K., Li, J., Murphy, C. A., Durham, M., et al. (2022). 3D bioassembly of cell-instructive chondrogenic and osteogenic hydrogel microspheres containing allogeneic stem cells for hybrid biofabrication of osteochondral constructs. *Biofabrication* 14, 034101. doi:10.1088/1758-5090/ac61a3

Fairbanks, B. D., Love, D. M., and Bowman, C. N. (2017). Efficient polymer-polymer conjugation via thiol-ene click reaction. *Macromol. Chem. Phys.* 218, 1700073. doi:10.1002/macp.201700073

Fairbanks, B. D., Scott, T. F., Kloxin, C. J., Anseth, K. S., and Bowman, C. N. (2009). Thiol-yne photopolymerizations: novel mechanism, kinetics, and step-growth formation of highly cross-linked networks. *Macromolecules* 42, 211–217. doi:10.1021/ma801903w

Fathollahipour, S., Patil, P. S., and Leipzig, N. D. (2018). Oxygen regulation in development: lessons from embryogenesis towards tissue engineering. *Cells Tissues Organs* 205, 350–371. doi:10.1159/000493162

Figueiredo, L., Le Visage, C., Weiss, P., and Yang, J. (2020). Quantifying oxygen levels in 3D bioprinted cell-laden thick constructs with perfusable microchannel networks. *Polym. (Basel)* 12, 1260. doi:10.3390/polym12061260

Figueiredo, L., Pace, R., D'Arros, C., Réthoré, G., Guicheux, J., Le Visage, C., et al. (2018). Assessing glucose and oxygen diffusion in hydrogels for the rational design of 3D stem cell scaffolds in regenerative medicine. *J. Tissue Eng. Regen. Med.* 12, 1238–1246. doi:10.1002/term.2656

Francis, S. L., Di Bella, C., Wallace, G. G., and Choong, P. F. M. (2018). Cartilage tissue engineering using stem cells and bioprinting technology—barriers to clinical translation. *Front. Surg.* 5, 70. doi:10.3389/fsurg.2018.00070

Greene, T., and Lin, C.-C. (2015). Modular cross-linking of gelatin-based thiol–norbornene hydrogels for *in vitro* 3D culture of hepatocellular carcinoma cells. *ACS Biomaterials Sci. Eng.* 1, 1314–1323. doi:10.1021/acsbiomaterials.5b00436

Gultice, A. D., Kulkarni-Datar, K., and Brown, T. L. (2009). Hypoxia-inducible factor 1alpha (HIF1A) mediates distinct steps of rat trophoblast differentiation in gradient oxygen. *Biol. Reprod.* 80, 184–193. doi:10.1095/biolreprod.107.067488

Hölzl, K., Fürsatz, M., Göcerler, H., Schädl, B., Žigon-Branc, S., Markovic, M., et al. (2022). Gelatin methacryloyl as environment for chondrocytes and cell delivery to superficial cartilage defects. *J. Tissue Eng. Regen. Med.* 16, 207–222. doi:10.1002/term.3273

Hoyle, C. E., and Bowman, C. N. (2010). Thiol–ene click chemistry. *Angew. Chem. Int. Ed.* 49, 1540–1573. doi:10.1002/anie.200903924

Hoyle, C. E., Lee, T. Y., and Roper, T. (2004). Thiol–enes: chemistry of the past with promise for the future. *J. Polym. Sci. Part A Polym. Chem.* 42, 5301–5338. doi:10.1002/pola.20366

Hoyle, C. E., Lowe, A. B., and Bowman, C. N. (2010). Thiol-click chemistry: a multifaceted toolbox for small molecule and polymer synthesis. *Chem. Soc. Rev.* 39, 1355–1387. doi:10.1039/b901979k

Huey, D. J., Hu, J. C., and Athanasiou, K. A. (2012). Unlike bone, cartilage regeneration remains elusive. *Science* 338, 917–921. doi:10.1126/science.1222454

Khurana, A., Liu, P., Mellone, P., Lorenzon, L., Vincenzi, B., Datta, K., et al. (2011). HSulf-1 modulates FGF2- and hypoxia-mediated migration and invasion of breast cancer cells. *Cancer Res.* 71, 2152–2161. doi:10.1158/0008-5472.can-10-3059

Klotz, B. J., Gawlitta, D., Rosenberg, A. J. W. P., Malda, J., and Melchels, F. P. W. (2016). Gelatin-methacryloyl hydrogels: towards biofabrication-based tissue repair. *Trends Biotechnol.* 34, 394–407. doi:10.1016/j.tibtech.2016.01.002

Lalitha Sridhar, S., Schneider, M. C., Chu, S., de Roucy, G., Bryant, S. J., and Vernerey, F. J. (2017). Heterogeneity is key to hydrogel-based cartilage tissue regeneration. *Soft matter* 13, 4841–4855. doi:10.1039/c7sm00423k

Lammi, M. J., Piltti, J., Prittinen, J., and Qu, C. (2018). Challenges in fabrication of tissue-engineered cartilage with correct cellular colonization and extracellular matrix assembly. *Int. J. Mol. Sci.* 19, 2700. doi:10.3390/ijms19092700

Lekvijittada, K., Hosomichi, J., Maeda, H., Hong, H., Changsiripun, C., Kuma, Y. i., et al. (2021). Intermittent hypoxia inhibits mandibular cartilage growth with reduced TGF-β and SOX9 expressions in neonatal rats. *Sci. Rep.* 11, 1140. doi:10.1038/s41598-020-80303-3

Leucht, A., Volz, A. C., Rogal, J., Borchers, K., and Kluger, P. J. (2020). Advanced gelatin-based vascularization bioinks for extrusion-based bioprinting of vascularized bone equivalents. *Sci. Rep.* 10, 5330. doi:10.1038/s41598-020-62166-w

Levato, R., Jungst, T., Scheuring, R. G., Blunk, T., Groll, J., and Malda, J. (2020). From shape to function: the next step in bioprinting. *Adv. Mater.* 32, 1906423. doi:10.1002/adma.201906423

Levett, P. A., Melchels, F. P., Schrobback, K., Hutmacher, D. W., Malda, J., and Klein, T. J. (2014). A biomimetic extracellular matrix for cartilage tissue engineering centered on photocurable gelatin, hyaluronic acid and chondroitin sulfate. *Acta Biomater.* 10, 214–223. doi:10.1016/j.actbio.2013.10.005

Lewis, P. L., Green, R. M., and Shah, R. N. (2018). 3D-printed gelatin scaffolds of differing pore geometry modulate hepatocyte function and gene expression. *Acta biomater.* 69, 63–70. doi:10.1016/j.actbio.2017.12.042

Li, S., Oreffo, R. O., Sengers, B. G., and Tare, R. S. (2014). The effect of oxygen tension on human articular chondrocyte matrix synthesis: integration of experimental and computational approaches. *Biotechnol. Bioeng.* 111, 1876–1885. doi:10.1002/bit.25241

Li, X., Chen, S., Li, J., Wang, X., Zhang, J., Kawazoe, N., et al. (2016). 3D culture of chondrocytes in gelatin hydrogels with different stiffness. *Polymers* 8, 269. doi:10.3390/polym8080269

Lim, K. S., Schon, B. S., Mekhileri, N. V., Brown, G. C. J., Chia, C. M., Prabakar, S., et al. (2016). New visible-light photoinitiating system for improved print fidelity in gelatin-based bioinks. *ACS Biomaterials Sci. Eng.* 2, 1752–1762. doi:10.1021/acsbiomaterials.6b00149

Lindberg, G. C. J., Cui, X., Durham, M., Veenendaal, L., Schon, B. S., Hooper, G. J., et al. (2021). Probing multicellular tissue fusion of cocultured spheroids-A 3D-bioassembly model. *Adv. Sci. (Weinh)* 8, e2103320. doi:10.1002/advs.202103320

Lobo, V., Patil, A., Phatak, A., and Chandra, N. (2010). Free radicals, antioxidants and functional foods: Impact on human health. *Pharmacogn. Rev.* 4, 118–126. doi:10.4103/0973-7847.70902

Lowe, A. B. (2014). Thiol-ene "click" reactions and recent applications in polymer and materials synthesis: a first update. *Polym. Chem.* 5, 4820–4870. doi:10.1039/c4py00339j

Lv, W., Zhou, H., Aazmi, A., Yu, M., Xu, X., Yang, H., et al. (2022). Constructing biomimetic liver models through biomaterials and vasculature engineering. *Regen. Biomater.* 9, rbac079. doi:10.1093/rb/rbac079

Magliaro, C., Mattei, G., Iacoangeli, F., Corti, A., Piemonte, V., and Ahluwalia, A. (2019). Oxygen consumption characteristics in 3D constructs depend on cell density. *Front. Bioeng. Biotechnol.* 7, 251. doi:10.3389/fbioe.2019.00251

Malda, J., Rouwkema, J., Martens, D. E., le Comte, E. P., Kooy, F. K., Tramper, J., et al. (2004). Oxygen gradients in tissue-engineered Pegt/Pbt cartilaginous constructs: measurement and modeling. *Biotechnol. Bioeng.* 86, 9–18. doi:10.1002/bit.20038

Martyniak, K., Lokshina, A., Cruz, M. A., Karimzadeh, M., Kemp, R., and Kean, T. J. (2022). Biomaterial composition and stiffness as decisive properties of 3D bioprinted constructs for type II collagen stimulation. *Acta Biomater.* 152, 221–234. doi:10.1016/j.actbio.2022.08.058

Mavris, S. M., and Hansen, L. M. (2021). Optimization of oxygen delivery within hydrogels. *J. Biomech. Eng.* 143, 101004. doi:10.1115/1.4051119

McCain, M. L., Agarwal, A., Nesmith, H. W., Nesmith, A. P., and Parker, K. K. (2014). Micromolded gelatin hydrogels for extended culture of engineered cardiac tissues. *Biomaterials* 35, 5462–5471. doi:10.1016/j.biomaterials.2014.03.052

Meng, W., Gao, L., Venkatesan, J. K., Wang, G., Madry, H., and Cucchiarini, M. (2019). Translational applications of photopolymerizable hydrogels for cartilage repair. *J. Exp. Orthop.* 6, 47. doi:10.1186/s40634-019-0215-3

Mouser, V. H., Melchels, F. P. W., Visser, J., Dhert, W. J. A., Gawlitta, D., and Malda, J. (2016). Yield stress determines bioprintability of hydrogels based on gelatin-methacryloyl and gellan gum for cartilage bioprinting. *Biofabrication* 8, 035003. doi:10.1088/1758-5090/8/3/035003

Nilasaroya, A., Poole-Warren, L. A., Whitelock, J. M., and Jo Martens, P. (2008). Structural and functional characterisation of poly(vinyl alcohol) and heparin hydrogels. *Biomaterials* 29, 4658–4664. doi:10.1016/j.biomaterials.2008.08.011

Occhetta, P., Visone, R., Russo, L., Cipolla, L., Moretti, M., and Rasponi, M. (2015). VA-086 methacrylate gelatine photopolymerizable hydrogels: a parametric study for highly biocompatible 3D cell embedding. *J. Biomed. Mater Res. A* 103, 2109–2117. doi:10.1002/jbm.a.35346

Pan, R. L., Martyniak, K., Karimzadeh, M., Gelikman, D. G., DeVries, J., Sutter, K., et al. (2022). Systematic review on the application of 3D-bioprinting technology in orthoregeneration: current achievements and open challenges. *J. Exp. Orthop.* 9, 95. doi:10.1186/s40634-022-00518-3

Peter, A., Hutmacher, D. W., Malda, J., and Klein, T. J. (2014). Hyaluronic acid enhances the mechanical properties of tissue-engineered cartilage constructs. *PLoS One* 9, e113216. doi:10.1371/journal.pone.0113216

Roberts, J. J., and Bryant, S. J. (2013). Comparison of photopolymerizable thiol-ene PEG and acrylate-based PEG hydrogels for cartilage development. *Biomaterials* 34, 9969–9979. doi:10.1016/j.biomaterials.2013.09.020

Rogers, N., and Meng, Q.-J. (2023). Tick tock, the cartilage clock. *Osteoarthr. Cartil.* 31, 1425–1436. doi:10.1016/j.joca.2023.05.010

Rouwkema, J., Koopman, B., Blitterswijk, C., Dhert, W., and Malda, J. (2010). Supply of nutrients to cells in engineered tissues. *Biotechnol. Genet. Eng. Rev.* 26, 163–178. doi:10.5661/bger-26-163

Schäfer, N., and Grässel, S. (2023). New refinements aim to optimize articular cartilage tissue engineering. *Nat. Rev. Rheumatol.* 19, 66–67. doi:10.1038/s41584-022-00889-y

Schmitz, C., Pepelanova, I., Ude, C., and Lavrentieva, A. (2022). Studies on oxygen availability and the creation of natural and artificial oxygen gradients in gelatin-methacryloyl hydrogel 3D cell culture. *J. Tissue Eng. Regen. Med.* 16, 977–986. doi:10.1002/term.3344

Schuurman, W., Levett, P. A., Pot, M. W., van Weeren, P. R., Dhert, W. J. A., Hutmacher, D. W., et al. (2013). Gelatin-methacrylamide hydrogels as potential biomaterials for fabrication of tissue-engineered cartilage constructs. *Macromol. Biosci.* 13, 551–561. doi:10.1002/mabi.201200471

Shepherd, D., and Seedhom, B. (1999). Thickness of human articular cartilage in joints of the lower limb. *Ann. Rheum. Dis.* 58, 27–34. doi:10.1136/ard.58.1.27

Soliman, B. G., Lindberg, G. C. J., Jungst, T., Hooper, G. J., Groll, J., Woodfield, T. B. F., et al. (2020). Stepwise control of crosslinking in a one-pot system for bioprinting of low-density bioinks. *Adv. Healthc. Mater.* 9, 1901544. doi:10.1002/adhm.201901544

Soliman, B. G., Longoni, A., Wang, M., Li, W., Bernal, P. N., Cianciosi, A., et al. (2023). Programming delayed dissolution into sacrificial bioinks for dynamic temporal control of architecture within 3D-bioprinted constructs. *Adv. Funct. Mater.* 33, 2210521. doi:10.1002/adfm.202210521

Sophia Fox, A. J., Bedi, A., and Rodeo, S. A. (2009). The basic science of articular cartilage: structure, composition, and function. *Sports Health* 1, 461–468. doi:10.1177/1941738109350438

Stampoultzis, T., Karami, P., and Pioletti, D. P. (2021). Thoughts on cartilage tissue engineering: a 21st century perspective. *Curr. Res. Transl. Med.* 69, 103299. doi:10.1016/j.retram.2021.103299

Starling, E. H. (1923). The anatomy and physiology of capillaries. *Nature* 112, 270–272. doi:10.1038/112270a0

Steele, J. A. M., Moore, A. C., St-Pierre, J. P., McCullen, S. D., Gormley, A. J., Horgan, C. C., et al. (2022). *In vitro* and *in vivo* investigation of a zonal microstructured scaffold for osteochondral defect repair. *Biomaterials* 286, 121548. doi:10.1016/j.biomaterials.2022.121548

Tijore, A., Irvine, S. A., Sarig, U., Mhaisalkar, P., Baisane, V., and Venkatraman, S. (2018). Contact guidance for cardiac tissue engineering using 3D bioprinted gelatin patterned hydrogel. *Biofabrication* 10, 025003. doi:10.1088/1758-5090/aaa15d

Tsai, C.-C., Kuo, S. H., Lu, T. Y., Cheng, N. C., Shie, M. Y., and Yu, J. (2020). Enzyme-Cross-linked gelatin hydrogel enriched with an articular cartilage extracellular matrix and human adipose-derived stem cells for hyaline cartilage regeneration of rabbits. *ACS Biomaterials Sci. Eng.* 6, 5110–5119. doi:10.1021/acsbiomaterials.9b01756

Visser, J., Levett, P. A., te Moller, N. C., Besems, J., Boere, K. W., van Rijen, M. H., et al. (2015). Crosslinkable hydrogels derived from cartilage, meniscus, and tendon tissue. *TISSUE Eng. Part A* 21, 1195–1206. doi:10.1089/ten.tea.2014.0362

Wang, B., Johnson, A., and Li, W. (2020). Development of an extracellular matrix-enriched gelatin sponge for liver wound dressing. *J. Biomed. Mater Res. A* 108, 2057–2068. doi:10.1002/jbm.a.36965

Wang, L.-S., Du, C., Toh, W. S., Wan, A. C., Gao, S. J., and Kurisawa, M. (2014). Modulation of chondrocyte functions and stiffness-dependent cartilage repair using an injectable enzymatically crosslinked hydrogel with tunable mechanical properties. *Biomaterials* 35, 2207–2217. doi:10.1016/j.biomaterials.2013.11.070

Yang, K.-H., Lindberg, G., Soliman, B., Lim, K., Woodfield, T., and Narayan, R. J. (2021). Effect of photoinitiator on precursory stability and curing depth of thiol-ene clickable gelatin. *Polymers* 13, 1877. doi:10.3390/polym13111877

Yue, K., Trujillo-de Santiago, G., Alvarez, M. M., Tamayol, A., Annabi, N., and Khademhosseini, A. (2015). Synthesis, properties, and biomedical applications of gelatin methacryloyl (GelMA) hydrogels. *Biomaterials* 73, 254–271. doi:10.1016/j.biomaterials.2015.08.045

Zavada, S. R., McHardy, N. R., and Scott, T. F. (2014). Oxygen-Mediated enzymatic polymerization of thiol–ene hydrogels. *J. Mater. Chem. B, Mater. Biol. Med.* 2, 2598–2605. doi:10.1039/c3tb21794a

Zhao, X., Lang, Q., Yildirimer, L., Lin, Z. Y., Cui, W., Annabi, N., et al. (2015). Photocrosslinkable gelatin hydrogel for epidermal tissue engineering. *Adv. Healthc. Mater* 5, 108–118. doi:10.1002/adhm.201500005

Zhou, S., Cui, Z., and Urban, J. P. (2004). Factors influencing the oxygen concentration gradient from the synovial surface of articular cartilage to the cartilage-bone interface: a modeling study. *Arthritis Rheum.* 50, 3915–3924. doi:10.1002/art.20675